

Supporting Information

The Protein Corona Inhibits Endosomal Escape of Functionalized DNA Nanostructures in Living Cells

Barbora Smolková^a, Tara MacCulloch^b, Tyler Rockwood^b, Minghui Liu^b, Skylar J.W. Henry^b, Adam Frtús^a, Mariia Uzhytchak^a, Mariia Lunova^{a,c}, Martin Hof^d, Piotr Jurkiewicz^d, Alexandr Dejneka^a, Nicholas Stephanopoulos^{b,}, and Oleg Lunov^{a,*}*

^a Department of Optical and Biophysical Systems, Institute of Physics of the Czech Academy of Sciences, Prague, 18221, Czech Republic

^b Biodesign Center for Molecular Design and Biomimetics, Arizona State University, Tempe, United States; School of Molecular Sciences, Arizona State University, Tempe, Arizona State University, Tempe, Arizona 85287, United States

^c Institute for Clinical & Experimental Medicine (IKEM), Prague, 14021, Czech Republic

^d J. Heyrovský Institute of Physical Chemistry of the Czech Academy of Sciences, Prague, 18223, Czech Republic

*Email: nstephal@asu.edu; lunov@fzu.cz

Table S1. Full sequences of the DNA strands that make up the 6-helix bundle DN. The colors correspond to the strands in Figure S1.

6HB-Blue	AGCGAACGTGGATTTTGTCCGACATCGGCAAGCTCCCTTTTTCGACTAT T
6HB-Green	CCGATGTCGGACTTTTACACGATCTTCGCCTGCTGGGTTTTGGGAGCTT G
6HB-Yellow	CGAAGATCGTGTTTTTCCACAGTTGATTGCCCTTCACTTTTCCCAGCAGG
6HB-Orange	AATCAACTGTGGTTTTTCTCACTGGTGATTAGAATGCTTTTGTGAAGGG C
6HB-Red	TCACCAGTGAGATTTTGTTCGTACCAGGTGCATGGATTTTGCATTCTA A
6HB-Purple	CCTGGTACGACATTTTCCACGTTTCGCTAATAGTCGATTTTATCCATGCA -Alexa Fluor 488

Table S2. Sequences of the synthesized peptides along with their expected masses. The observed mass was obtained using MALDI-MS, the spectra are displayed in Figure S2.

Peptide	Amino Acid Sequence	Expected Mass
K10	KKKKKKKKKK	1298.75
K10 with fluorescein	Fluorescein-KKKKKKKKKK	1657.05
K10 with pHrodo	KKKKKKKKKKC-pHrodo Red	≈2108.9 *
EE-K10	GLFDIHKIAESFGSGKKKKKKKKKKGSGFEAIKKIIDF LG	4626.65
EE scramble-K10	IKAFKGFDESILIGSGKKKKKKKKKKGSGILISEDGKF AKI	4626.65

(* the pHrodo dye from the supplier was reported as a mass of “~700” Da, so this value was used to calculate the expected mass of the peptide-dye conjugate)

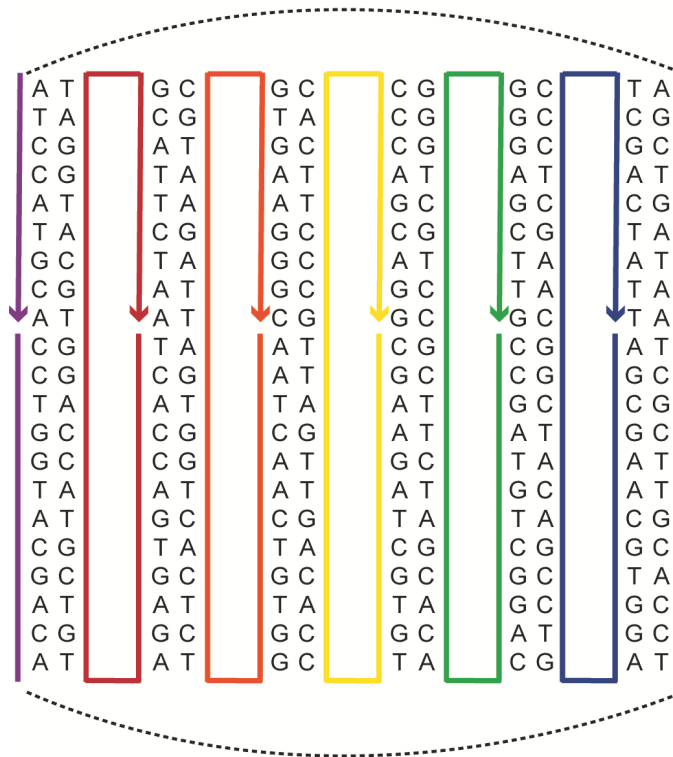


Figure S1. Topology diagram showing the sequence and connectivity of the 6 strands (each colored differently) that make up the 6-helix bundle DNA nanostructure. Each strand has four thymine in the linking regions between the duplexes.

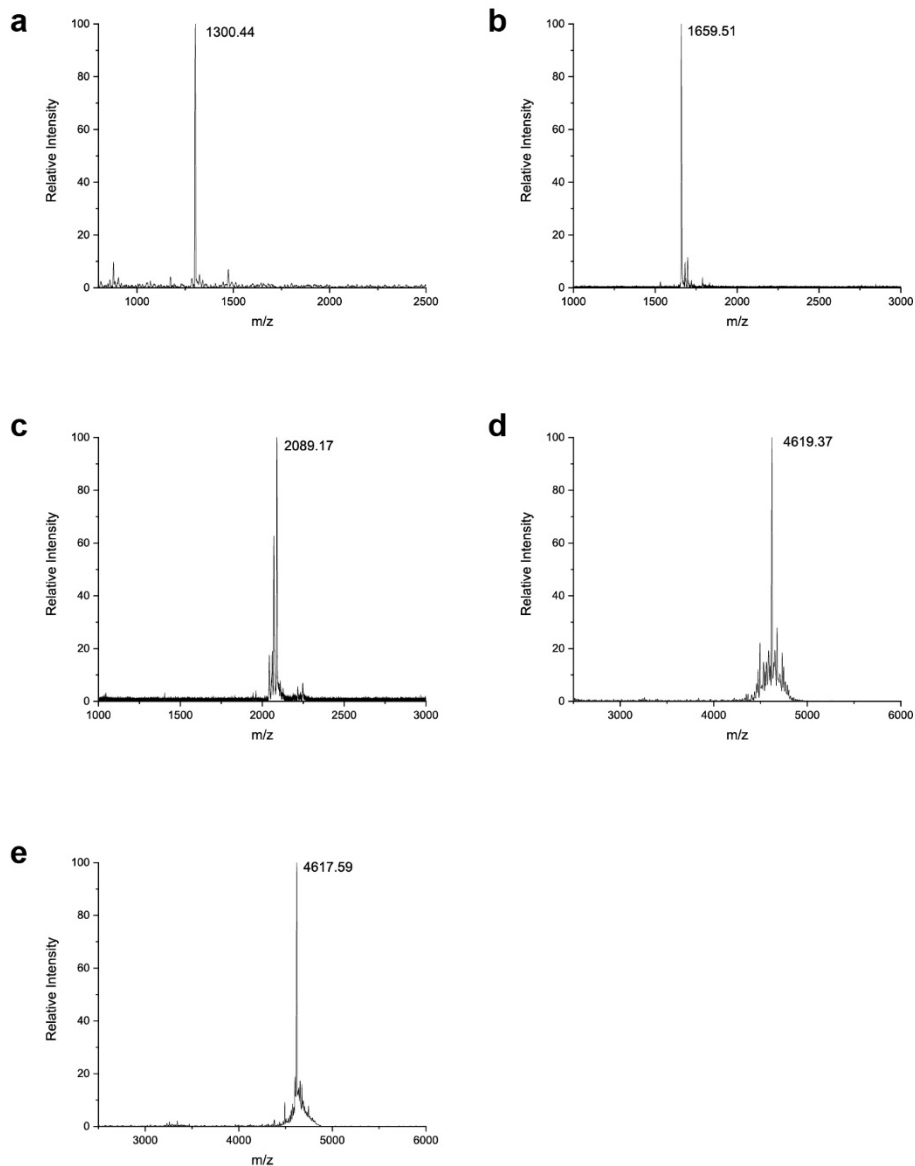


Figure S2. MALDI-TOF mass spectra of the indicated purified peptides. All mass values are given in Da. (a) Plain K10 with an observed mass of 1300.4 and an expected mass of 1298.8. (b) K10-fluorescein with an observed mass of 1657.1 and an expected mass of 1659.5. (c) pHrodo labeled K10 with an observed mass of 2089.2 and an expected mass of approximately 2108.9. (d) EE-K10 with an observed mass of 2619.4 and an expected mass of 4626.7. (e) EE-K10 scramble with an observed mass of 2617.6 and an expected mass of 4626.7.

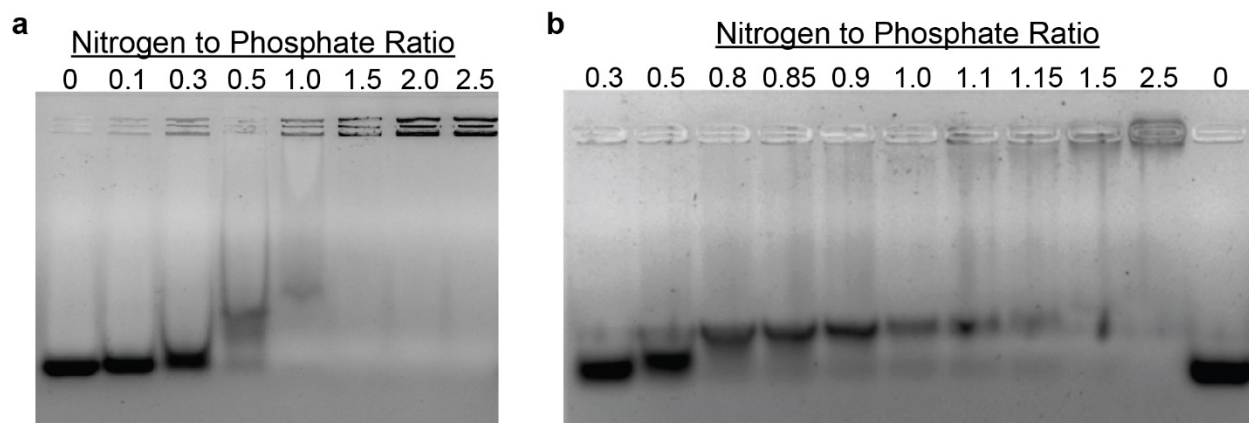


Figure S3. (a) Agarose gel electrophoresis (1.5% agarose) used to determine the integrity of the 6 helix bundle as well as the optimal nitrogen to phosphate (N:P) ratio in order to fully coat (via electrostatic neutralization) the DNA nanostructure. (b) Optimization of the N:P ratio around 0.8-1.5. For all experiments, the ratio of N:P = 1 was used; below this value the DNs did not show a complete gel shift, and increasing the peptide coating beyond this level yielded aggregation.

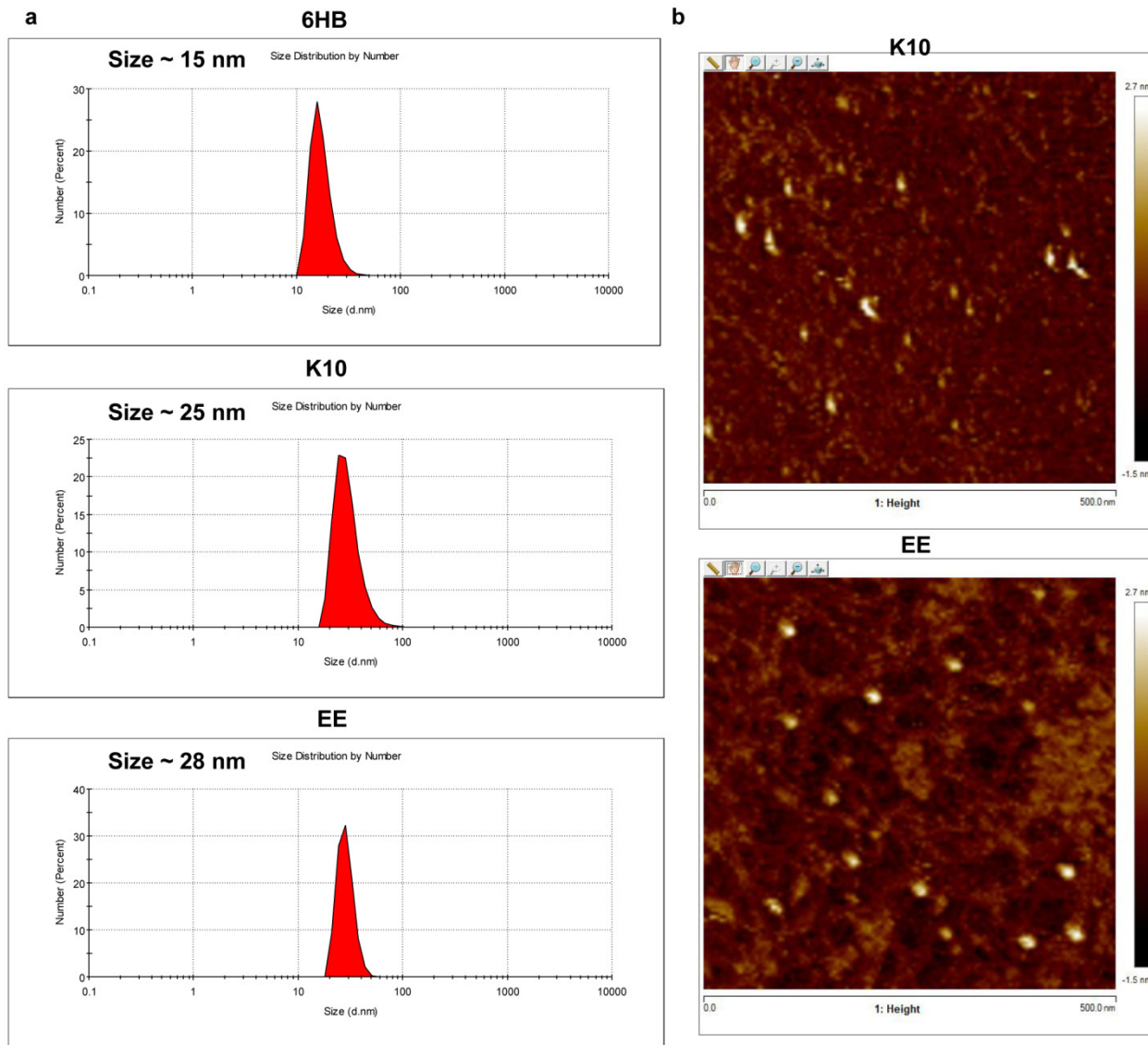


Figure S4. (a) Size distribution of different DNs. Characterization of the particles dissolved in PBS measured with a Zetasizer Nano (Malvern Instruments). (b) AFM characterization of the K10 and EE DNs.

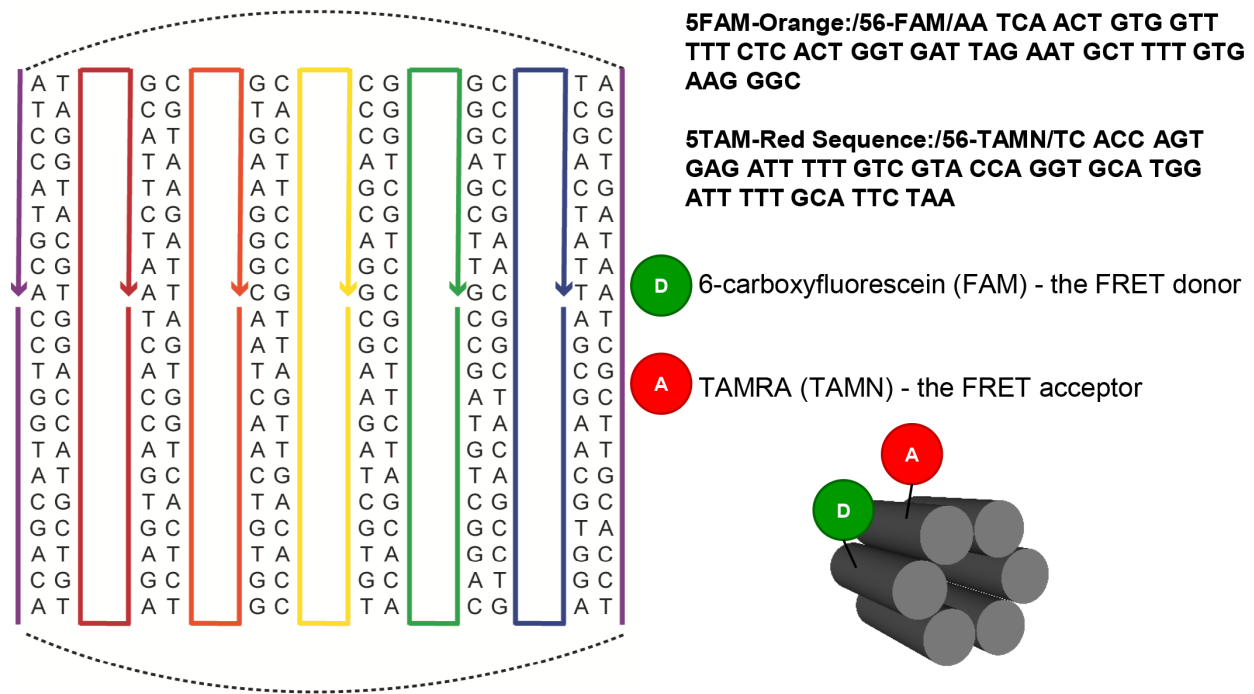


Figure S5. FRET-based monitoring of DNA nanostructure stability. Schematic representation of the 6HB structure labelled with FRET reporter dyes. Two selected staples are modified with FRET donor (6-carboxyfluorescein, green circle) and acceptor (TAMRA, red circle) dyes, respectively.

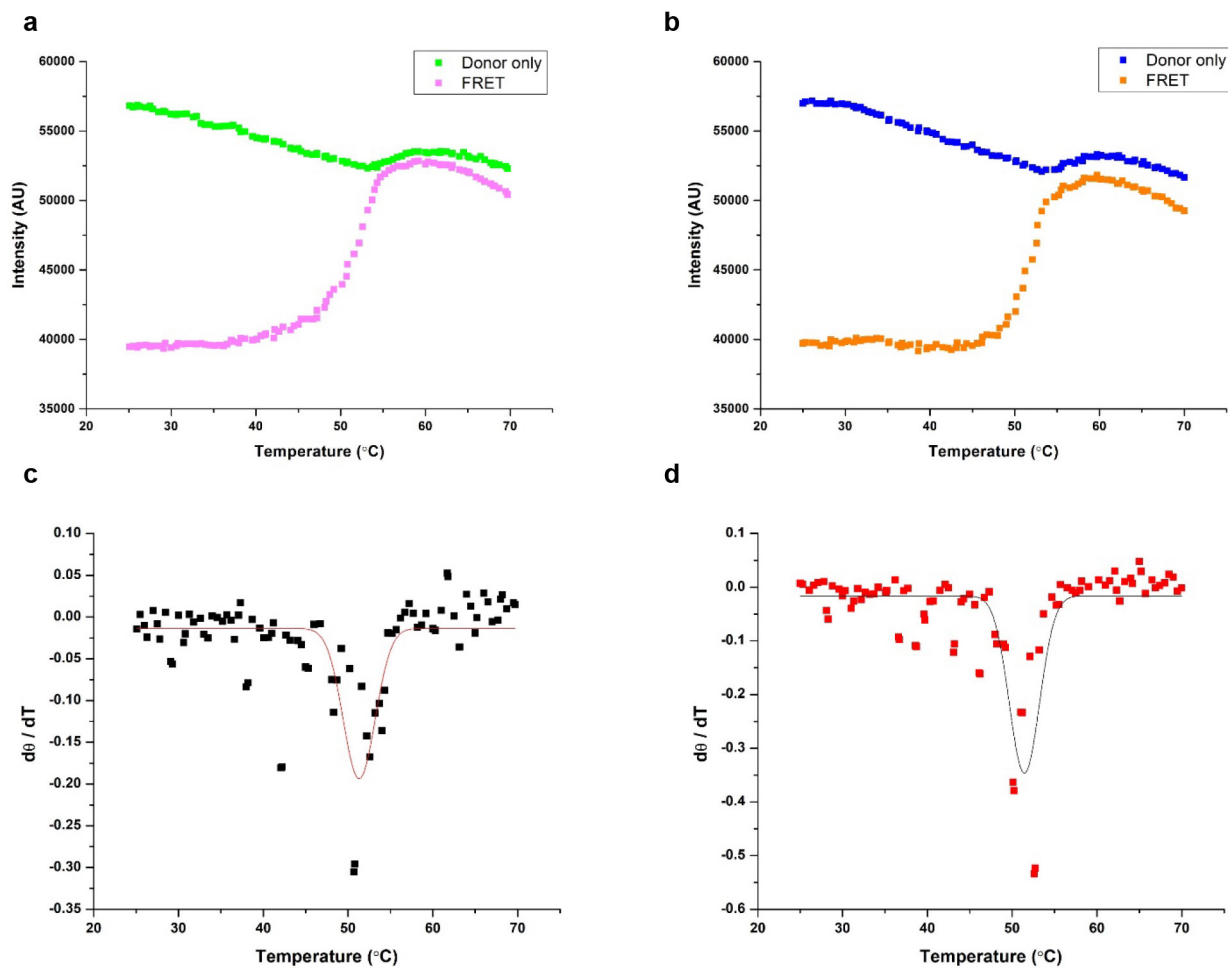


Figure S6. FRET-based monitoring of DNA nanostructure stability of freshly prepared 6HB. (a) Raw fluorescent intensity versus temperature for the cooling cycle. (b) Raw fluorescent intensity versus temperature for the heating cycle. (c) The derivative of the cooling curve and corresponding Gaussian fit to yield the transition temperature of folding, T_f . (d) The derivative of the heating curve and corresponding Gaussian fit to yield the transition temperature of melting, T_m .

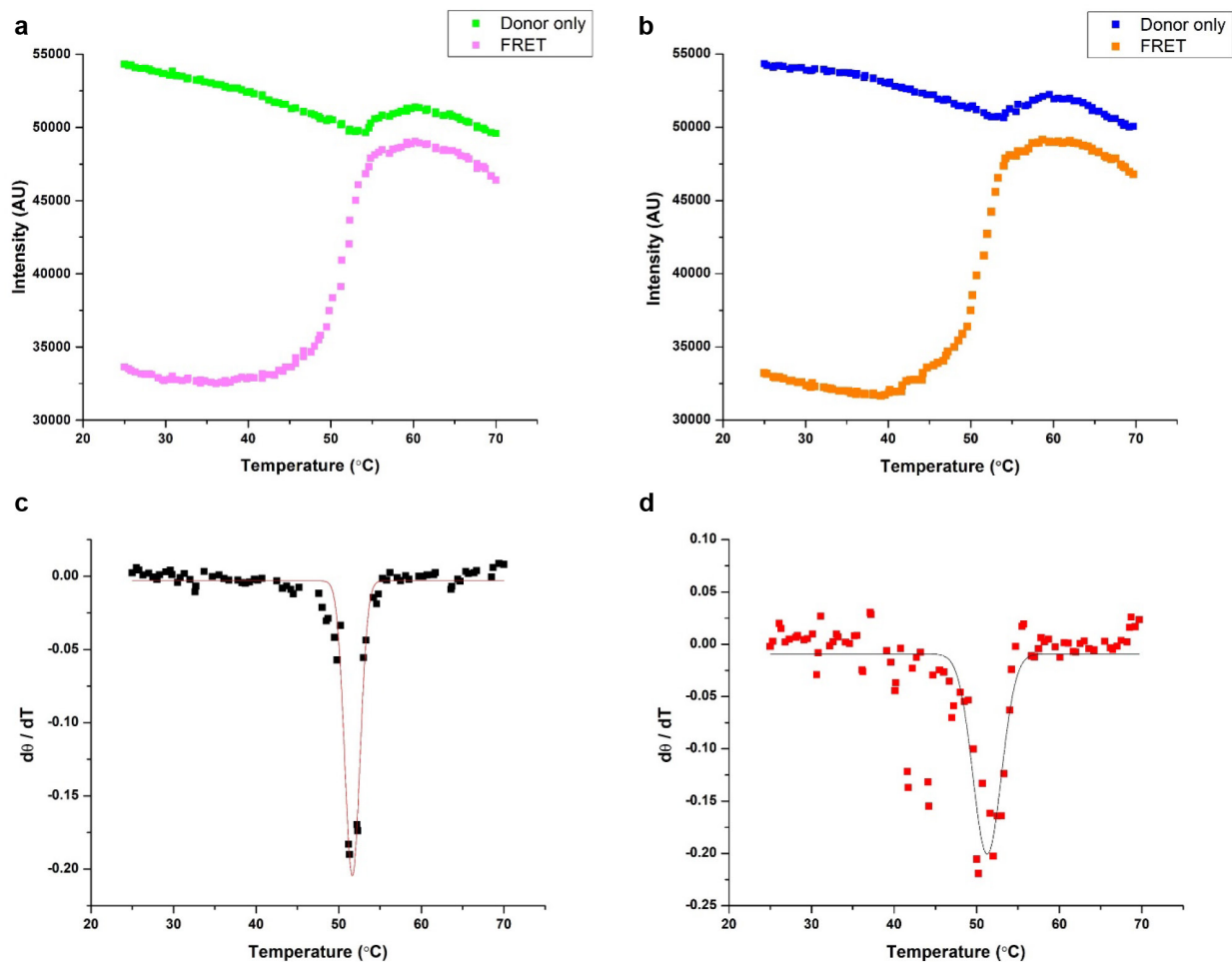


Figure S7. FRET-based monitoring of DNA nanostructure stability of 6HB incubated at room temperature for 2 days. (a) Raw fluorescent intensity versus temperature for the cooling cycle. (b) Raw fluorescent intensity versus temperature for the heating cycle. (c) The derivative of the cooling curve and corresponding Gaussian fit to yield the transition temperature of folding, T_f . (d) The derivative of the heating curve and corresponding Gaussian fit to yield the transition temperature of melting, T_m .

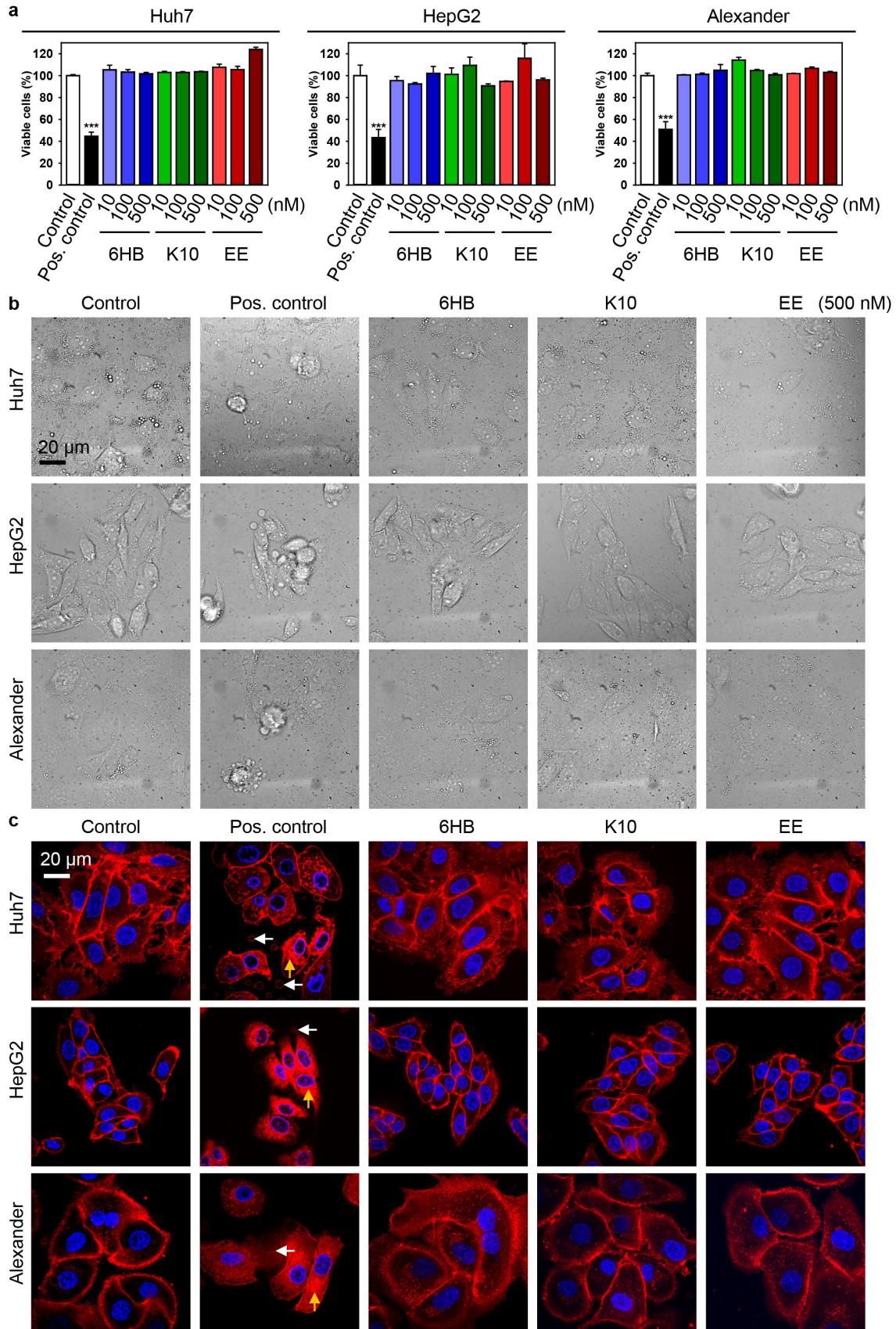


Figure S8. Assessment of DN's biocompatibility in three distinct hepatic cell lines. (a) Cytotoxicity of nanoparticles in three distinct cell lines: Alexander, HepG2, Huh7. Cells were treated with different DN's (10, 100 and 500 nM) for 24 h. Cytotoxicity was assessed using alamarBlue assay. The data were normalized to control values (no particle exposure), which were set as 100% cell viability. Control cells were untreated. As a positive control, cells were treated with 20% ethanol for 60 min. Data are expressed as means \pm SEM (n = 3). (b) Cells were treated with different DN's (500 nM) for 24 h. After treatment DIC images were acquired using inverted microscope IX83 (Olympus, Tokyo, Japan). As a positive control, cells were treated with 20% ethanol for 15 min. (c) Cells were treated with different DN's for 24 h. After treatment, cells were labelled with CellMask™ Orange (Thermo Fisher Scientific) plasma membrane stain. Stained cells were imaged using spinning disk confocal microscopy IXplore SpinSR (Olympus, Tokyo, Japan). Representative images out of three independent experiments are presented. As a positive control, cells were treated with 20% ethanol for 15 min. Yellow arrows indicate cell membrane rupture as evident by cytosolic dye accumulation; white arrows show vesicles shedding.

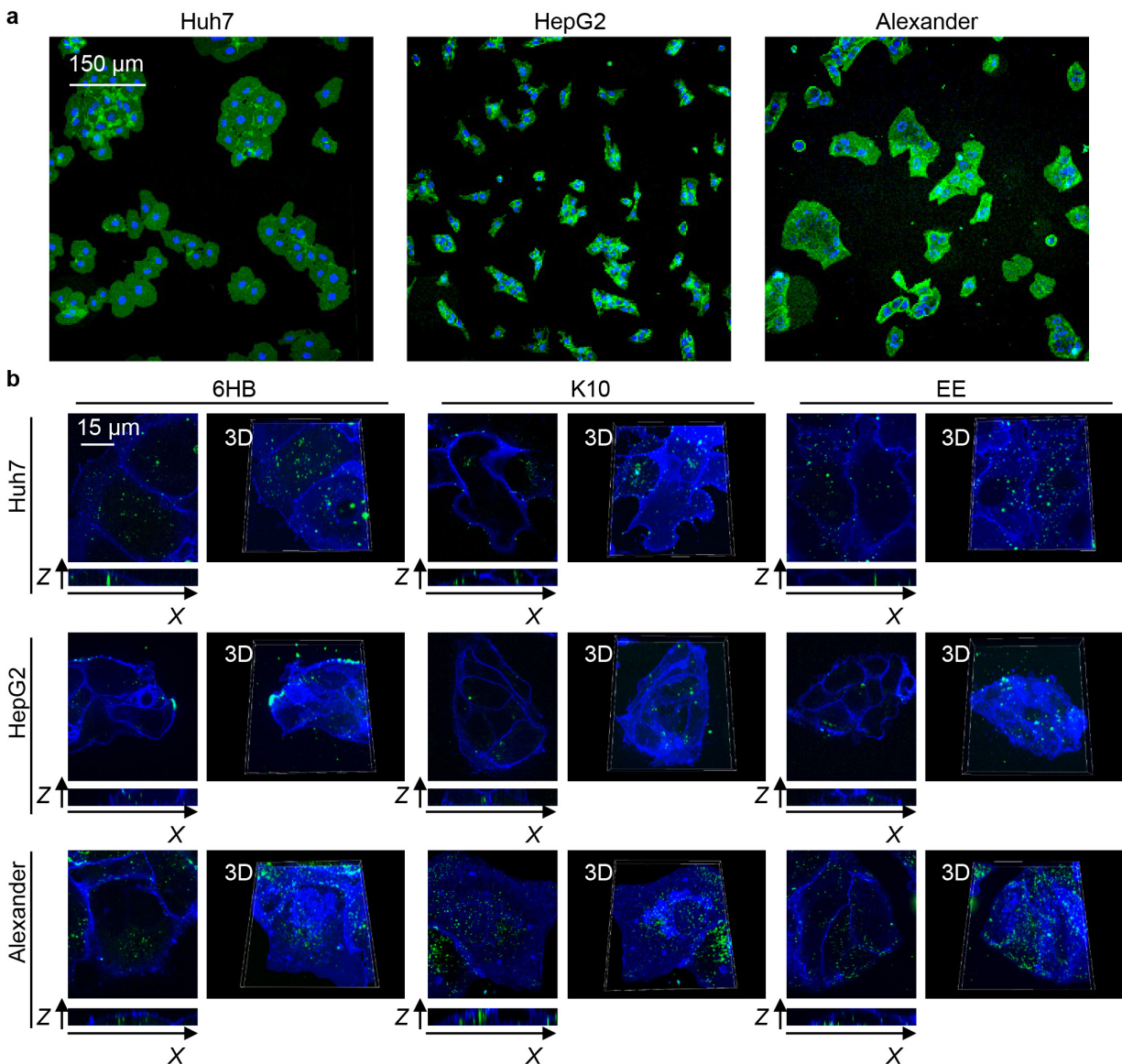


Figure S9. Uptake of different DNAs by three distinct hepatic cell lines. (a) Assessment of cell size and morphology in Huh7, HepG2 and Alexander cells. Cells were stained with CellMask™ Green (Thermo Fisher Scientific) plasma membrane stain. Nuclei were counterstained with Hoechst 33342 (Thermo Fisher Scientific). Stained cells were imaged using spinning disk confocal microscopy IXplore SpinSR (Olympus, Tokyo, Japan). Representative images out of three independent experiments are presented. (b) Alexander, HepG2, Huh7 cell lines were treated with 50 nM concentration of different fluorescently-labeled (green fluorescence) DNAs for

24 h. After treatment, cells were fixed with 4% Paraformaldehyde (VWR) and labelled with CellBrite™ Blue (Biotium) plasma membrane stain. Stained cells were imaged using spinning disk confocal microscopy IXplore SpinSR (Olympus, Tokyo, Japan). 3D rendering orthogonal projections were done using ImageJ software (NIH). Representative images out of three independent experiments are presented.

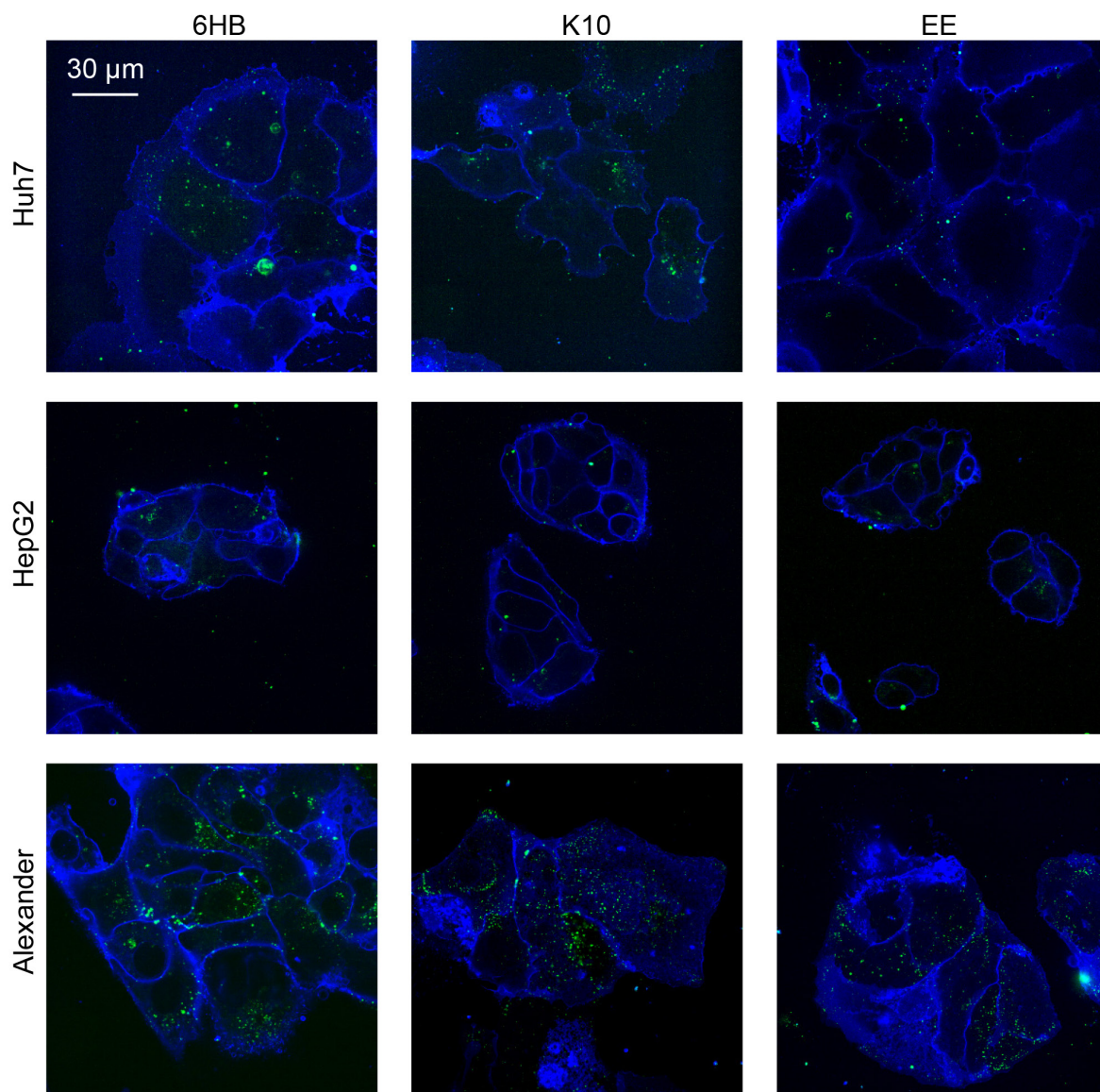


Figure S10. Assessment of DN uptake in three distinct hepatic cell lines. Alexander, HepG2, Huh7 cell lines were treated with 50 nM concentration of different DN for 24 h. After treatment, cells were labelled with CellBrite™ Blue (Biotium) plasma membrane stain. Stained cells were imaged using spinning disk confocal microscopy IXplore SpinSR (Olympus, Tokyo, Japan). Representative images out of three independent experiments are presented.

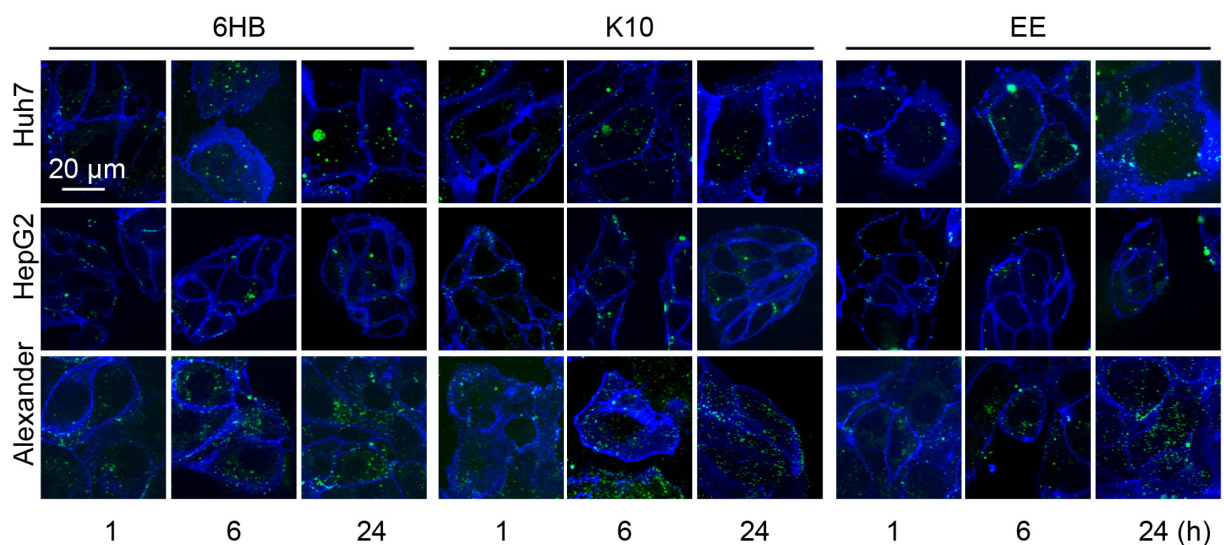


Figure S11. Assessment of DN uptake kinetics in three distinct hepatic cell lines. Alexander, HepG2, Huh7 cell lines were treated with 50 nM concentration of different DN for 1, 6 and 24 h. After treatment, cells were labelled with CellBrite™ Blue (Biotium) plasma membrane stain. Stained cells were imaged using spinning disk confocal microscopy IXplore SpinSR (Olympus, Tokyo, Japan). Representative images out of three independent experiments are presented.

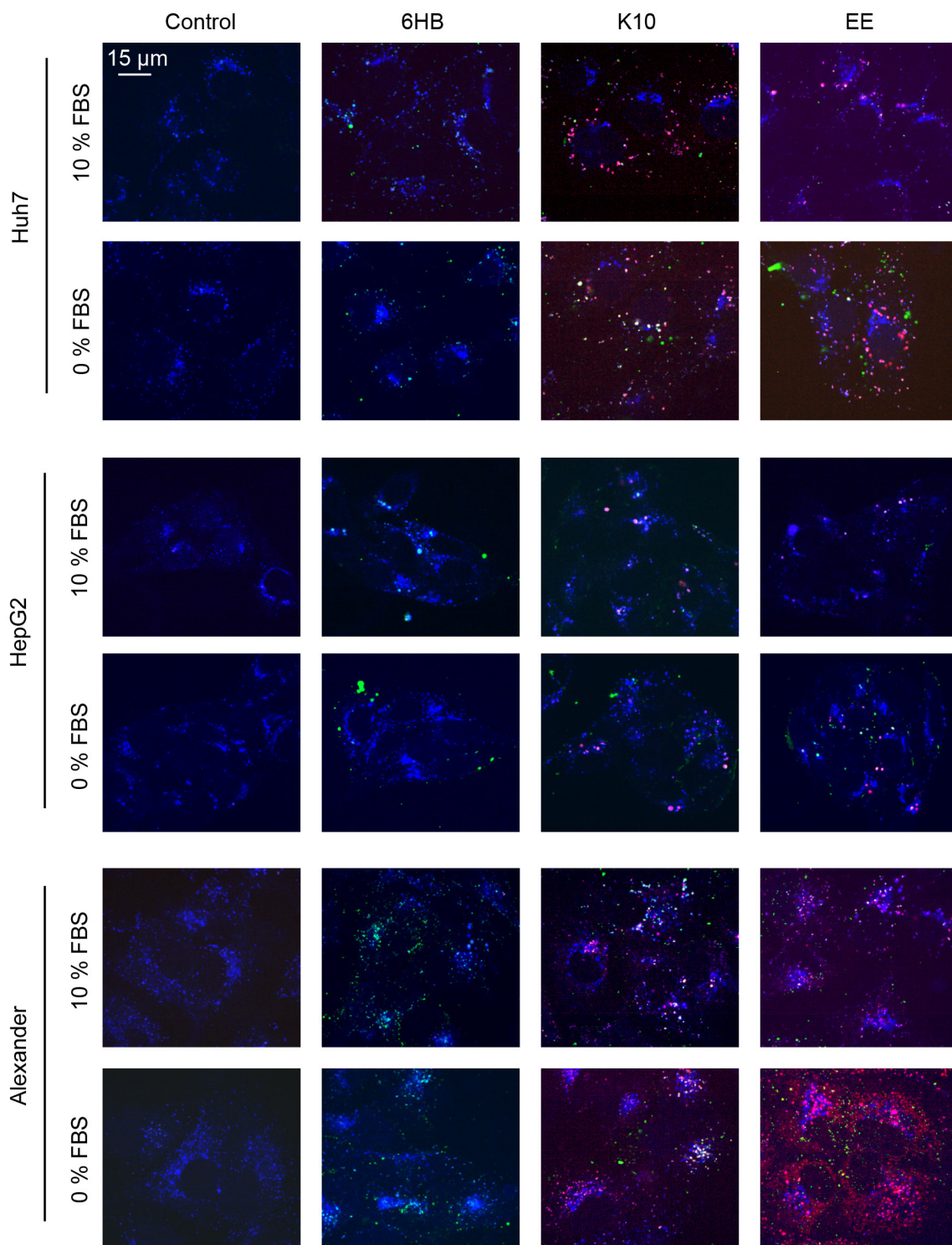


Figure S12. Colocalization assessment of DNs in three distinct hepatic cell lines. Alexander, HepG2, Huh7 cell lines were treated with 50 nM concentration of different DNs for 6 h either in

full medium (10 % FBS EMEM) or in serum-free medium (0 % FBS EMEM). After incubation cells were labelled with lysosomal marker LysoTracker® Blue DND-22 (Thermo Fisher Scientific). Stained cells were imaged using spinning disk confocal microscopy IXplore SpinSR (Olympus, Tokyo, Japan). Representative images out of three independent experiments are presented. K10 and EE DNs possess pHrodo (red) dye. DNA of all DNs was labelled with Alexa-488.

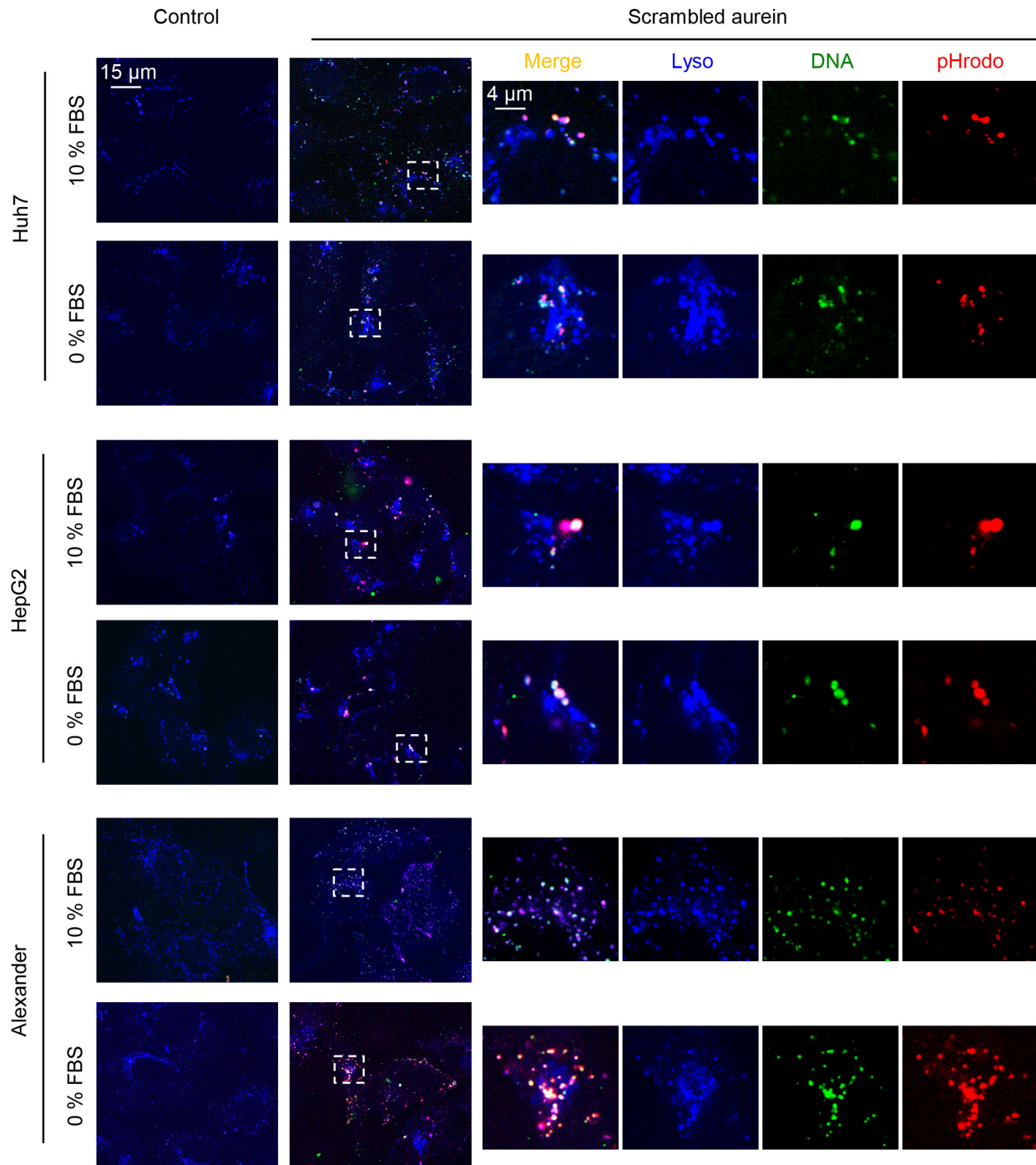


Figure S13. Colocalization assessment of scrambled aurein-decorated DNPs in three distinct hepatic cell lines. Alexander, HepG2, Huh7 cell lines were treated with 50 nM concentration of different DNPs for 6 h either in full medium (10 % FBS EMEM) or in serum-free medium (0 %

FBS EMEM). After incubation cells were labelled with lysosomal marker LysoTracker® Blue DND-22 (Thermo Fisher Scientific). Stained cells were imaged using spinning disk confocal microscopy IXplore SpinSR (Olympus, Tokyo, Japan). Representative images out of three independent experiments are presented. DNs possess pHrodo (red) dye. DNA of DNs was labelled with Alexa-488.

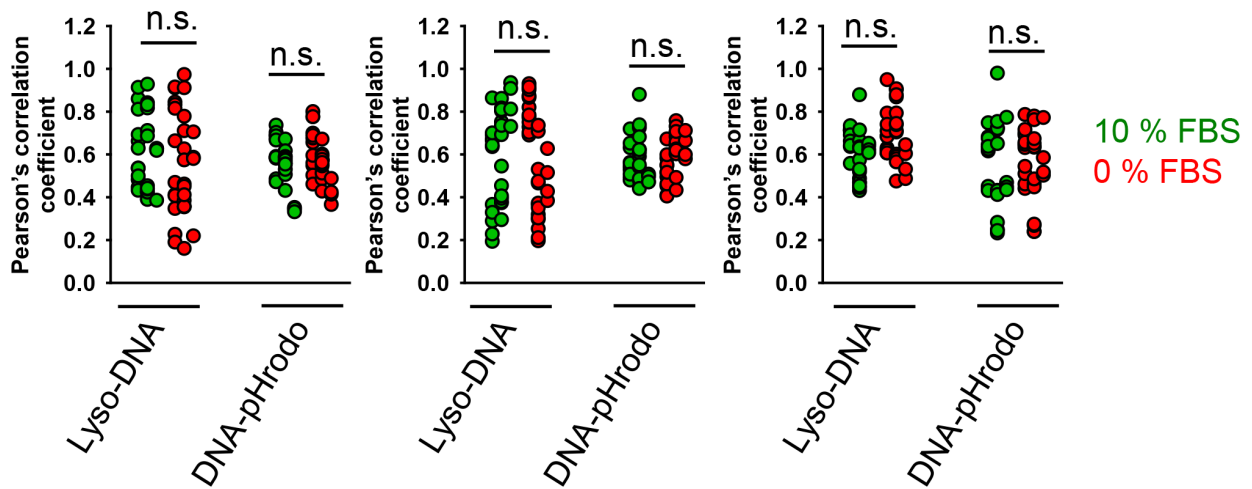


Figure S14. Pearson's correlation coefficient for fluorophore pairs either DNA-Lysosomes or DNA-pHrodo was calculated using Coloc 2 tool available in ImageJ software (NIH) and presented as means of $n = 30$ cells.